JOURNAL OF GEOPHYSICAL RESEARCH, VOL. 106, NO. C5, PAGES 9117–9133, MAY 15, 2001

A sea ice climate switch mechanism for the 100-kyr glacial cycles

Hezi Gildor and Eli Tziperman

Environmental Sciences, Weizmann Institute, Rehovot, Israel

Abstract. A box model of the ocean-atmosphere-sea ice-land ice climate system is used to study a novel mechanism for self-sustained oscillations of the climate system on a time scale of 100,000 years, without external forcing. The oscillation in land ice volume has the familiar sawtooth shape of climate proxy records. The most novel aspect of the climate oscillations analyzed here is the crucial role played by the sea ice. The sea ice acts as a "switch" of the climate system, switching it from a growing land glaciers mode to a retreating land glaciers mode and shaping the oscillation's sawtooth structure. A simple explanation of the 100-kyr timescale is formulated on the basis of the mechanism seen in the model. Finally, rapid sea ice changes such as those seen in our model, and their drastic effects on the climate system, may provide an explanation to some of the rapid climate changes observed to be a part of the variability at all timescales in the paleorecord.

1. Introduction

Earth's climate undergoes variations on a wide range of timescales, from seasonal and interannual to glacial-interglacial and beyond, as can be seen in a variety of proxy records from ice cores, ocean sediments, and other sources [*Kerr*, 1998; *Bender et al.*, 1997; *GRIP-Greenland Ice-Core Projects Members*, 1993]. Some of the more distinctive features in these records are a pronounced timescale of 100,000 years (100 kyr), with additional weaker spectral peaks at 40, 20, and 10 kyr, and an asymmetric sawtooth structure (the slow buildup of the land glaciers and the relatively abrupt melting) as can be seen, for example, in marine records of $\delta^{18}O$ [*Imbrie et al.*, 1984] or in ice core records [*Petit et al.*, 1999; *Bender et al.*, 1997]. The (weak) consensus is that the variability on the timescale of 100 kyr resulted from nonlinear self-sustained internal oscillations of the climate system (possibly relaxation oscillations) paced by orbital forcing (see reviews by *Imbrie et al.* [1993], *Crowley and North* [1991], *Ghil* [1994], *Saltzman* [1990], and *Imbrie et al.* [1992] and references therein). External forcing such as volcanism and changes in solar activity may have acted to modulate or randomize these internal oscillations but are thought to be too weak to account for the observed amplitude of the 100-kyr variability. In spite of much progress, it is probably fair to state that the source of the dominant 100-kyr timescale, the typical asymmetric sawtooth pattern of glacial-interglacial climatic variability, and the mechanism of observed rapid climate transitions [*Lehman and Keigwin*, 1992; *Bender et al.*, 1997] still lack a satisfactory detailed physical mechanism [*Raymo*, 1998].

There have been several proposed mechanisms for the 100-kyr timescale. A nonlinear transfer of energy from the Milankovitch forcing at higher frequencies to the 100-kyr timescale was invoked by *Le Treut and Ghil* [1983]. Isostatic adjustments of the lithosphere under the weight of the glacier [*Oerlemans*, 1982] was also suggested as a source of the 100-kyr cycle, although this adjustment is generally believed now to be too fast to account for the 100-kyr cycle (yet too slow to account for the rapid climate transitions observed in proxy records). *Saltzman and Sutera* [1984] obtained 100-kyr cycles with the sawtooth structure in a model representing ice sheets, adjoining marine ice and ocean. *Saltzman and Maasch* [1988] obtained a 100-kyr cycle due to a parameterized feedback between the ice sheets, ocean and atmospheric CO_2. *Watts and Hayder* [1984] used an energy balance model (EBM) coupled to an ice sheet model. They have postulated an enhanced ice sheet collapse during deglaciation through glacier calving due to the rising of sea level and obtained a 100-kyr cycle.

Rapid climate transitions seen in the paleorecord often last less than a few decades. This was previously explained by instabilities of the thermohaline circulation [*Broecker and Denton*, 1989; *Paillard*, 1998] or by ice sheet instabilities [*Pollard*, 1983; *Watts and Hayder*, 1984; *Imbrie et al.*, 1993]. General circulation models (GCM) [*Manabe et al.*, 1991; *Manabe and Stouffer*, 1988; *Tziperman*, 1997; *Rind et al.*, 1989] and simpler models [*DeBlonde and Peltier*, 1993; *Peltier and Marshall*, 1995] show that a thermohaline circulation (THC) instability or multiple equilibria do not have the global

Paper number 1999JC000120.
0148-0227/01/1999JC000120$09.00

effect that is likely to explain glacial-interglacial transitions. Similarly, *Peltier and Marshall* [1995] concluded that marine-based ice sheet instability was unable to induce rapid glacial termination in their coupled EBM/ice sheet climate model. *Gallée et al.* [1992] found that a specified decrease in the albedo of aging snow during deglaciation induced rapid glacial termination in their model. Similarly, *Peltier and Marshall* [1995] attributed the rapid deglaciation to albedo variations due to dust loading. A satisfactory detailed mechanism of the rapid climate transitions is still missing.

The models used in order to understand the variability of Earth's climate system range from simple energy balance models coupled to ice sheet models [*Weertman*, 1976; *Pollard et al.*, 1980; *Watts and Hayder*, 1984; *Ghil*, 1994; *Birchfield et al.*, 1994; *Peltier and Marshall*, 1995; *Sakai and Peltier*, 1997; *Suarez and Held*, 1976] through intermediate models [*Ganopolski et al.*, 1998; *Weaver et al.*, 1998] and up to general circulation models [*Manabe and Broccoli*, 1985; *Kutzbach and Guetter*, 1986; *Rind et al.*, 1989; *Bush and Philander*, 1998]. Owing to their large computer time requirements, GCMs have been used only for simulating ice age climate as an equilibrium response to prescribed glacial conditions and orbital parameters. The time-dependent nonequilibrium response of the climate system and the mechanism of onset or termination of an ice age are therefore often investigated by using much simpler models which enable the investigation of lag effects and nonlinear interactions between the climate system components. These simple model studies helped to elucidate the role of many processes in the climate system.

In this paper we use a simple zonally averaged box model of the ocean-atmosphere-sea ice-land ice climate system to propose a novel mechanism for climate oscillations on a timescale of the order of 100 kyr, with an asymmetric sawtooth structure and without external (i.e., Milankovitch) forcing. We also propose a simple derivation for the 100-kyr timescale based on the proposed oscillation mechanism. The model includes representations of the ocean meridional thermohaline circulation, the atmospheric temperature and humidity feedback, the land glaciers, and the sea ice. The glacial-interglacial oscillations in our model occur owing to the combination of the ice albedo and a variant of the precipitation-temperature feedback [*Källén et al.*, 1979; *Ghil et al.*, 1987; *Ghil*, 1994]. The precipitation-temperature feedback suggests that the increase in accumulation rate of snow over land glaciers due to a temperature increase outweighs the corresponding increase in ablation and melting. Indeed, many proxy records show an increase in accumulation rate during warmer periods [*Cuffey and Clow*, 1997; *Alley et al.*, 1993; *Lorius et al.*, 1979]. It is more difficult to estimate the effect of temperature increase on the rate of ablation, as it is very difficult to evaluate the terms contributing to the mass balance of an ice sheet even for present-day climate [*Paterson*, 1994]. Modeling studies of the response of the Antarctic ice sheet to greenhouse warming suggest that for a temperature increase of up to 5.3°C from present-day temperatures, the increased accumulation still dominates the increase in ablation [*Huybrechts and Oerlemans*, 1990]. The Greenland ice sheet seems more sensitive to global warming, but for colder climate than today's, the precipitation-temperature feedback is expected to work there as well [*Huybrechts et al.*, 1991, Figure 3]. Other studies suggest that this feedback may also work in the context of future warming due to CO_2 increase [*Miller and de Vernal*, 1992; *Ledley and Chu*, 1994].

Previous model studies using atmospheric GCMs [*Krinner and Genton*, 1998; *Charles et al.*, 1994; *Hall et al.*, 1996] as well as proxy records [*Kapsner et al., 1995*] have shown that the change in accumulation rate over land glacier are a result of a combination of the temperature effect on the moisture holding capacity of the air and atmospheric circulation changes. A significant part of the precipitation (20%) on the glaciers (Greenland, for example) comes locally from the Norwegian and Greenland seas [*Charles et al.*, 1994]. Further studies of proxy records have shown that such temperature and atmospheric circulation changes may have occurred over a very short period of less than 20 years and suggest that rapid change of the sea ice cover in the North Atlantic Ocean may have been the cause of these changes [*Dansgaard et al.*, 1989; *Taylor et al.*, 1993]. Furthermore, very recent proxy records show that sea ice has extended during the last glacial maximum as far south as 45°N-50°N in the North Atlantic Ocean, which is a much more extensive cover than that of present day [*de Vernal and Hillaire-Marcel*, 2000]. This extensive sea ice cover during the last glacial maximum is critical in affecting the atmospheric circulation as hinted in the above proxy and model studies not only due to its extensive area coverage, but also due to its location near the glaciers of North America and northern Europe. Finally, the evidence on the extensive sea ice coverage during the last glacial maximum is not restricted to the North Atlantic Ocean, but also includes the North Pacific Ocean [*de Vernal and Pedersen*, 1997] which may also have controlled the transport of humidity to the North American glaciers.

The most novel and crucial aspect of the mechanism proposed here for the glacial-interglacial cycles involves the major role played by the sea ice, in accordance with the above proxy and atmospheric GCM evidence. The sea ice in our model acts as a "switch" of the climate system, switching it from a growing land ice mode to a retreating land ice mode and shaping the oscillation's structure. This is done through the effects of the sea ice on snow accumulation over land glaciers, via the sea ice effects both on the atmospheric meridional moisture transport and on the evaporation from the high-latitude ocean. The proposed mechanism resembles the "moisture initiators" climate theories [*Ruddiman and McIntyre*, 1984; *Stokes*, 1955; *Donn and Ewing*, 1966; *Rud-*

diman and McIntyre, 1981], according to which climate changes are caused by variations in the atmospheric moisture flux to high-latitude land masses. *Ruddiman and McIntyre* [1981] suggested that an increase of summer insolation has started the deglaciations, which in turn caused a flow of cold water into the ocean, resulting in an increased sea ice cover. In our mechanism, in contrast, the creation of sea ice precedes the deglaciation, and Milankovitch forcing is not needed for the oscillation to exist. Some previous simple dynamical models were able to fit available proxy records quite well [e.g., *Saltzman and Sutera*, 1984; *Paillard*, 1998]. The present model, being more detailed, represents more explicitly the dynamics and interaction between different components of the climate system. It therefore predicts a more detailed and specific sequence of events which can be verified or falsified by using new sea ice proxies that are expected to be available in the near future.

It should be clear that the purpose of the model used in this paper, being highly idealized and neglecting zonal variations, is only to explore a limited set of feedbacks rather than produce a realistic simulation of the glacial cycles. The model fails to reproduce, for example, the synchronous deglaciation of the Southern Hemisphere, and the temperature variations are not necessarily in full agreement with available proxies. Numerous physical feedbacks are ignored and others are rather poorly represented. In spite of these obvious shortcomings of our idealized model, we feel this model has captured some potentially important and interesting feedbacks of the sea ice role in the glacial-interglacial cycles. The take-home message of this model study is that sea ice feedbacks may act as climate switches and may participate in shaping some of the features of the observed past climate variability. In a subsequent paper [*Gildor and Tziperman*, 2000] we take into account the effects of seasonality in particular and of the variation of other orbital parameters in general (Milankovitch forcing). We demonstrate there that while the seasonal and orbital forcings can pace the 100 kyr oscillation in our model and make it more realistic looking, they do not change its mechanism as presented and analyzed in this paper. It is therefore important to understand that the seasonality and Milankovitch forcing are not responsible for the 100-kyr oscillation mechanism we propose here, and one of the objectives of the present paper is to demonstrate this explicitly.

The outline of this paper is as follows. Section 2 describes the model, section 3 is devoted to analyzing the glacial oscillation mechanism and to formulating a simple argument for the 100-kyr timescale. The model sensitivity to its key parameters is presented in section 4, and we conclude in section 5.

2. Model Description

Our coupled meridional box model, schematically shown in Figure 1, is composed of ocean, atmosphere, sea ice, and land ice models. The ocean model (section 2.1) includes four surface boxes and four deep boxes and represents both hemispheres. The two polar boxes represent the regions between 45° and the poles, while the two midlatitude boxes include the regions between the equator and 45°. The polar boxes may be covered with sea ice of a variable extent (section 2.1). The atmospheric model (section 2.2) is divided into four boxes, representing the same latitude bands as the ocean boxes. Each atmospheric box may have four types of lower surfaces: ocean, land, land ice, and sea ice, each with its specified albedo. The land part in the polar boxes may be covered by glaciers of a variable area (section 2.3). All model parameters are given in Table 1. All prognostic equations are solved by a leapfrog scheme in time, using a uniform time step for all variables. A Robert time filter with $\gamma = 0.25$ has

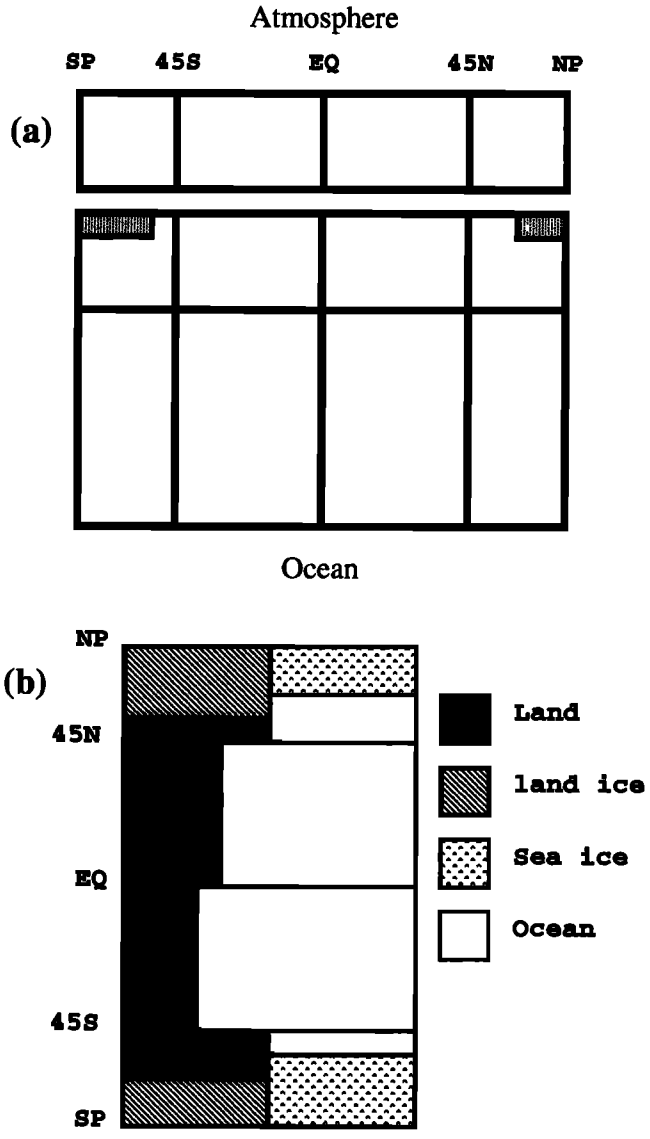

Figure 1. Box model (a) meridional cross section with shaded regions representing sea ice cover; (b) top view.

Table 1. Parameters Used in the Model

Parameter, Units	Value
Ocean Model	
$L_1, \cdot\cdot, L_4$, $10^6\ m$	4.15, 10., 10., 4.15
r, s^{-1}	$3. \times 10^{-4}$
ρ_0, $kg\,m^{-3}$	1028.
K_h, $m^2\,s^{-1}$	3.5×10^{-4}
K_v, $m\,s^{-1}$	4.2×10^{-8}
D_{upper}, m	400
D_{lower}, m	4000
τ, s	8.7×10^7
C_{pw}, $J\,kg^{-1}\,^\circ K$	4180.
Sea ice Model	
$D_{\text{sea-ice}}$, m	2.
γ, m	0.05
C_{pw}, $J\,kg^{-1}\,K^{-1}$	4180.
$\rho_{\text{sea-ice}}$, $kg\,m^{-3}$	917.
$\tau_{\text{sea-ice}}$, s	2.6×10^6
L_f, $J\,kg^{-1}$	3.34×10^5
Atmospheric Model	
$W_1, \cdot\cdot, W_4$, $10^7\ m$	1.8, 1.8, 1.8, 1.8
$f_{L1}, \cdot\cdot, f_{L4}$	0.5, 0.2, 0.35, 0.5
$\alpha_{\text{land-ice}}$, $\alpha_{\text{sea-ice}}$, α_{land}, α_{ocean}, α_{cloud}	0.85, 0.65, 0.20, 0.07, 0.30
R, $J\,Kg^{-1}\,K^{-1}$	287.04
C_p, $J\,Kg^{-1}\,K^{-1}$	1004.
Q_S, $W\,m^{-2}$	342.
$P_{lw1}, \cdot\cdot, P_{lw4}$	0.58, 0.56, 0.54, 0.626
K_θ, $s^{-1}\,K^{-2}$	15.5×10^{20}
K_{Mq}, $m^4\,s^{-1}\,K^{-1}$	5.4×10^{13}
K_q, $m^3\,s^{-1}$	3.3×10^8
A, Pa	2.53×10^{11}
B, K	5.42×10^3
Land ice Model	
LI_{Sink4}, Sv	0.076

been used in order to suppress the leapfrog $2\Delta T$ mode [*Haltiner and Williams*, 1980].

2.1. Ocean and Sea Ice Models

The ocean model is a fairly standard meridional box model similar to those used in many previous studies [*Stommel*, 1961; *Tziperman et al.*, 1994]. The north-south lengths of the oceanic boxes $(L_1, \cdots, L_4)$ are the same as those of the atmospheric boxes above them. The width of the ith ocean box is $(1 - f_{Li})W_i$, where f_{Li} and W_i are the land fraction and width of the ith atmospheric box. The thickness of the upper ocean boxes is D_{upper}, while that of the lower ones is D_{lower}. The model dynamics include a simple frictional horizontal momentum balance and are hydrostatic and mass conserving. Advection and diffusion of temperature and salinity are balanced by surface fluxes. The equation of state is the full nonlinear equation recommended by *UNESCO* [1981]. Under these assumptions, the continuous governing equations become

$$0 = -\frac{1}{\rho_0}P_z - \frac{g}{\rho_0}\rho \quad (1)$$

$$0 = -\frac{1}{\rho_0}P_y - rv \quad (2)$$

$$0 = v_y + w_z \quad (3)$$

$$T_t + (vT)_y + (wT)_z = K_h T_y + K_v T_z + Q_T^{\text{atm}} + Q_T^{\text{sea-ice}} \quad (4)$$

$$S_t + (vS)_y + (wS)_z = K_h S_y + K_v S_z + Q_S^{\text{atm}} + Q_S^{\text{sea-ice}} + Q_S^{\text{land-ice}} \quad (5)$$

The finite difference form is like that of *Tziperman et al.* [1994]. In the above equations, (y, z) and (v, w) are the (northward, upward) coordinates and velocities; P denotes pressure; T and S are ocean temperature and salinity, respectively; g is gravitational acceleration; ρ_0 is a constant reference water density; r is a friction coefficient; K_h and K_v are the horizontal and vertical diffusion coefficients, respectively. Whenever the vertical stratification is unstable, the vertical diffusion coefficient is made about 300 times larger than its value for stable stratification (this larger value gives a mixing time of 1 year for the upper polar box under unstable stratification; the value for K_v in Table 1 is for stable stratification).

Q_T^{atm} is the heat flux between the atmosphere and the ocean due to sensible, latent heat and radiative fluxes. A *Haney* [1971] type parameterization is used for this flux component over open ocean water, and the insulat-

ing effect of sea ice of a thickness $D_{\text{sea-ice}}$ is included as well [*Walsh*, 1982], so that

$$Q_T^{\text{atm}} = \frac{\rho_0 C_{pw} D_{\text{upper}}}{\tau}(\theta - T)\left\{f_{ow} + f_{si}\frac{\gamma}{D_{\text{sea-ice}}}\right\}, \quad (6)$$

where θ is the atmospheric potential temperature and C_{pw} is the heat capacity of ocean water. The parameter τ which has the dimension of time is chosen such that the heat transport to the northern polar atmospheric box by the ocean is around 2.3 PW during an interglacial period; f_{ow} and f_{si} are the fractions of open water and sea ice cover in the box, such that $f_{ow} = 1 - f_{si}$. The parameter γ represents the insulating effect of the sea ice.

The freshwater forcing at the ocean surface is translated into an equivalent salt flux used to drive the ocean salinity equation

$$Q_S^{\text{atm}} = -(P - E)S_0, \quad (7)$$

where $P-E$ is the precipitation minus evaporation (section 2.2) and S_0 is a constant reference salinity.

The heat and equivalent salt fluxes due to the formation or melting of sea ice are given by $Q_T^{\text{sea-ice}}$ and $Q_S^{\text{sea-ice}}$ in (4) and (5). When the temperature of the water in the polar boxes drops below a specified critical temperature, $T^{\text{sea-ice}}$, sea ice is formed. The heat flux available then for the formation of sea ice is calculated by using a simple relaxation term using a short timescale $\tau_{\text{sea-ice}}$,

$$Q_T^{\text{sea-ice}} = \frac{\rho_0 C_{\text{pw}} V_{\text{ocean}}}{\tau_{\text{sea-ice}}}(T^{\text{sea-ice}} - T), \quad (8)$$

where V_{ocean} is the volume of the oceanic box. When the ocean temperature rises above $T^{\text{sea-ice}}$ and sea ice is present, the available heat based on the same expression is used to melt the sea ice. The short timescale used in the sea ice melting/freezing term ensure that the ocean temperature remains very near (fraction of a degree) to the freezing temperature as long as sea ice is present. Sea ice thus melts/forms when the ocean temperature is just slightly above/below the freezing point. The heat flux $Q_T^{\text{sea-ice}}$ is converted into the amount of sea ice created or melted, by dividing it by $\rho_{\text{sea-ice}} L_f$, where $\rho_{\text{sea-ice}}$ is the density of sea ice and L_f is the latent heat of fusion. The equation for the sea ice volume is therefore

$$\frac{d(V_{\text{sea-ice}})}{dt} = \frac{Q_T^{\text{sea-ice}}}{\rho_{\text{sea-ice}} L_f} + P_{\text{on-ice}},$$

where $V_{\text{sea-ice}}$ is the volume of sea ice in the box and $P_{\text{on-ice}}$ is the amount of sea ice buildup due to atmospheric precipitation on the part of the ocean covered with sea ice. Initially, as sea ice starts forming, its thickness is assumed constant (1.5 m and 2 m in the southern and northern polar boxes, respectively) until all the box is covered with sea ice. As part of the sensitivity tests, we show that the model is not sensitive to the specified thickness, as the main effects of sea ice are its albedo and its insulating effect. In the experiments presented below, the sea ice never covers the entire box area. The formation and melting of sea ice in our model also affect the salinity budget (5), through an equivalent salt flux,

$$Q_S^{\text{sea-ice}} = \frac{Q_T^{\text{sea-ice}}}{\rho_{\text{sea-ice}} L_f} S_0,$$

which represents brine rejection due to sea ice formation or freshwater flux due to sea ice melting. Finally, $Q_S^{\text{land-ice}}$ in (5) is the equivalent salinity flux due to ablation of land ice under the same atmospheric box (section 2.3).

The dominant effect of the sea ice albedo feedback in the Southern Ocean resulted in a fully sea ice cover in the Southern Ocean when the ocean covers 80% of the box area (the same proportion as in the real world). This occurred because a sea ice growth leads to a significantly increased albedo, therefore to atmospheric cooling, and thus to further sea ice growth, until the Southern Ocean box is fully sea ice covered (ice albedo feedback). Some negative mechanisms should exist in the real world in order to allow partially covered state. Possible mechanisms are enhanced vertical mixing, wind-induced upwelling, and topographic effects, which are missing in our simple model. A too high sensitivity to the sea ice albedo feedback is common among many models, including general circulation models [*Ingram et al.*, 1989]. We therefore have followed the example of previous studies and have artificially increased the land fraction in the southern box from 20% to 50% [e.g., *Hasumi*, 1997]. This decreases the ocean area and therefore weakens the sea ice albedo effect and keeps the sea ice from covering the entire box area.

2.2. Atmospheric Model

The atmospheric model roughly follows the models of *Marotzke and Stone* [1995], *Rivin and Tziperman* [1997], and *Kagan et al.* [1984]. The dimensions of the atmospheric boxes and the land fractions are similar to those used by *Birchfield et al.* [1982]. The averaged potential temperature of each box is calculated on the basis of the energy balance of the box, taking into account (1) incoming solar radiation (as in the case of *North and Coakley* [1979]) using box albedo calculated according to the relative fraction of each lower surface type in the box, (2) outgoing longwave radiation at the top of the atmosphere, (3) air-sea heat flux, and (4) meridional atmospheric heat transport.

The heat equation in pressure coordinates is

$$C_p T \frac{d \ln \theta}{dt} = Q,$$

where Q is the heating rate per unit mass and $\theta = T(P_0/P)^{\frac{R}{C_p}}$ is the potential temperature at pres-

sure P, relative to a reference pressure P_0; T is the air temperature; R is the gas constant for dry air; and C_p is the specific heat of the atmosphere at a constant pressure. From the heat equation in pressure coordinates we find $d\theta/dt = (1/C_P)\theta T^{-1}Q$. Taking the box model potential temperature to represent the potential temperature at $500\,mbar$ and letting the reference level be $P_0 = 1000\,mbar$, we get $\theta/T = 2^{R/C_p}$ so that $d\theta/dt = 2^{R/C_p}Q/C_p$. Expressing the heating rate as the divergence of a heat flux, F, such that $Q = -(1/\rho)\nabla \cdot F$ and integrating the heat equation over the volume of an atmospheric box, we obtain

$$\frac{\partial\theta}{\partial t} = \frac{2^{R/C_p}g}{P_0C_p} * \left[(F_{\text{Top}} - F_{\text{Surface}}) + (F^{\text{in}}_{\text{merid}} - F^{\text{out}}_{\text{merid}})\right], \quad (9)$$

where F_{Top} and F_{Surface} are the heat fluxes at the top of the atmosphere and at the surface, respectively, and where $F^{\text{in}}_{\text{merid}} - F^{\text{out}}_{\text{merid}}$ is the net heating due to the meridional heat flux between the atmospheric boxes. Equation (9) is the averaged (over the box area a) heat balance for a column of air extending from the surface to the top of the atmosphere, with a cross section of $1\,m^2$. Over land and land ice we assume no net heat flux into the surface; so F_{Surface} is only the heat flux between the ocean and the atmosphere, Q^{atm}_T.

F_{Top} is composed of the incoming solar radiation H_{in}, between the latitudes ϕ_1 and ϕ_2 which define the atmospheric box boundaries, and the outgoing longwave radiation H_{out}, for a box with a mean potential temperature θ:

$$F_{\text{Top}} = H_{\text{in}} - H_{\text{out}} \quad (10)$$

$$H_{\text{in}} = (1-\alpha_{\text{surface}})(1-\alpha_{\text{cloud}})R_E^2 * \int_{\phi_1}^{\phi 2} Q_S \cos\phi d\phi d\lambda \quad (11)$$

$$H_{\text{out}} = P_{lw}\sigma\theta^4, \quad (12)$$

where R_E is the radius of the Earth, α_{cloud} is a specified constant cloud albedo, and α_{surface} is the box albedo which is calculated according to relative fraction and the specified albedo of each surface type (α_{land}, $\alpha_{\text{land-ice}}$, α_{ocean}, and $\alpha_{\text{sea-ice}}$ for land, land ice, ocean, and sea ice, respectively). The albedo of each surface type is assumed independent of time, neglecting, for example, the differences between the albedo of old and new ice [*Gallée et al.*, 1992] or the zenith angle dependence. Q_S is the solar constant divided by four; σ is the Stefan-Boltzmann constant, and P_{lw} is an emissivity coefficient which in principle depends on humidity, cloud cover, land cover and topography, aerosol, CO_2 concentration, etc., and is therefore allowed here to vary from box to box. P_{lw} is taken here to be constant in time, neglecting temporal variations of atmospheric humidity, CO_2, and the aerosol concentrations. In principle, one expects the emissivity to increase from glacial minima to glacial maxima owing to the reduced water vapor concentration. Similarly, it may be expected that the cloud cover is larger during interglacial periods, and thus the cloud albedo should be larger at such times. The precise dependencies of the emissivity and cloud albedo on the atmospheric temperature and humidity are clearly unknown at this time, and we chose to assume that the two effects cancel exactly, which is equivalent to assuming constant emissivity and cloud albedo as we did. In the current paper we force the model with annual mean solar radiation, ignoring seasonal and orbital variations. In a subsequent paper [*Gildor and Tziperman*, 2000], we take into account the effects of seasonality in particular and of the variation of other orbital parameters in general (Milankovitch forcing). We demonstrate there that while the seasonal and orbital forcing pace the 100-kyr oscillation, they do not change its mechanism as presented and analyzed in this paper.

For the meridional heat transport F_{merid} we use [*Chen et al.*, 1995]

$$F_{\text{merid}} = K_\theta \nabla\theta, \quad (13)$$

where K_θ is chosen such that the meridional heat transport by the atmosphere between the two northern boxes during an interglacial period is about 2.2 PW, close to the present-day observed value [*Peixoto and Oort*, 1992]. In finite difference form, the meridional heat flux between boxes 2 and 3, for example, takes the form

$$F_{\text{merid}} = K_\theta \frac{(\theta_2 - \theta_3)}{0.5\,(L_2 + L_3)}.$$

Rather than using humidity as a prognostic variable, we assume constant relative humidity of 0.7 [*Manabe and Strickler*, 1964], so that $q = 0.7q_s$ and the saturation humidity q_s at a temperature T is calculated from an approximate Clausius-Clapeyron equation

$$q_s = A * e^{B/T}.$$

The meridional atmospheric moisture transport, F_q, plays an important role in the temperature-precipitation feedback which, in turn, is responsible for the glacial-interglacial oscillations in our model. As was mentioned above, proxy records [*Cuffey and Clow*, 1997; *Alley et al.*, 1993; *Lorius et al.*, 1979] and GCMs [*Charles et al.*, 1994] clearly show that snow accumulation over high-latitude glaciers is increased during warm periods, sometimes by a factor of 4 and up to an order of magnitude. This is probably the result of both temperature changes and changes in the atmospheric circulation (such as southward shift of the storm track [e.g., *Hall et al.*, 1996; *Ganopolski et al.*, 1998]).

Given the importance of the meridional atmospheric moisture flux, we have run the model with several possible parameterizations for it. The most common choice of $F_{Mq} = K_{Mq}|\nabla\theta|\nabla q$ [*Stone*, 1972] was found inappropriate for studying the glacial-interglacial cycle:

when entering a glacial period, the meridional temperature gradient strengthens significantly, and the humidity decreases; but the relatively small change in ∇q is dominated by the large increase in $\nabla\theta$, such that the poleward humidity flux increases rather than decreases in a cold period. The alternative $F_{Mq} = F_{\text{merid}}\partial q/\partial T$, where F_{merid} is the meridional atmospheric heat transport (similar to *Chen et al.*, [1995]), based on a linearization of the humidity-temperature relation, is appropriate for studying present-day climate variability and even tends to increase the meridional moisture flux during warm periods due to the nonlinearity of the Clausius-Clapeyron equation. It seems, however, that the physical mechanism of the temperature-precipitation feedback should be related to the available atmospheric humidity [*Robin*, 1977] rather than to the nonlinearity of the Clausius-Clapeyron equation. Consequently, we chose to parameterize the meridional atmospheric moisture transport as

$$F_{Mq} = K_{Mq}\,|\nabla\theta|\,q, \tag{14}$$

where q is the humidity of the box to which the humidity flux is directed and the constant K_q is chosen such that the meridional water transport between the two northern boxes during an interglacial is about 0.38 Sv, close to the present-day value [*Schmitt*, 1994]. The flux is down the gradient of absolute humidity (determined in the model uniquely by the temperature, as relative humidity being assumed constant). This parameterization brings into account both the meridional temperature gradient which controls the strength of synoptic scale motions and hence also the eddy moisture fluxes and, more important, the ability of the box receiving the moisture flux to actually hold and carry this moisture. Note that if the temperature of the polar box is very low (glacial period), its humidity q is correspondingly low, and the box is not expected to be able to carry the humidity flux from the boundary with the midlatitude box toward the polar areas where the land glaciers are. The freshwater flux between the boxes, transported by atmospheric eddies, will therefore not be able to cross the border between the midlatitude and polar boxes. This effect is represented in (14) through the factor q of the atmospheric box receiving the moisture flux.

The details of this parameterization are clearly not easily justifiable on physical grounds, but note also that the more commonly used parameterizations could not produce the observed changes in snow accumulation at high latitude during warm periods and therefore cannot reproduce the glacial oscillations in our box model. Because of the limitations of simple models such as the present one (e.g., the zonal averaging and lack of atmospheric dynamics), one needs to resort to such crude and somewhat less justified choices. Perhaps future studies with atmospheric GCMs will lead to a better box model parameterization of the temperature precipitation feedback.

Results of GCMs [*Charles et al.*, 1994] and some proxy records [*Hebbeln et al.*, 1994] indicate that a significant amount of the precipitation feeding the glaciers comes from high latitudes (as the Norwegian and Greenland seas). Therefore another source of precipitation over the land ice sheets in the polar boxes is local evaporation from the part of the polar box ocean not covered by sea ice, parameterized by

$$F_q = K_q f_{ow} q. \tag{15}$$

The presence of sea ice during cold periods significantly reduces this source of moisture, as the fraction of open water ocean, f_{ow}, becomes small, weakening the source of land ice sheets growth. This effect complements the temperature-precipitation feedback and the effect of the sea ice on the atmospheric circulation which reduces the moisture supply to the glaciers during periods of extensive sea ice cover. The parameterization (15) is added, as we feel it is consistent with the above proxy and model studies, although glacial oscillations exist in our model even without it. The local evaporation and resulting local precipitation over land in the midlatitude ocean boxes (as opposed to over land ice in the polar boxes) is assumed to be compensated by runoff to the same ocean box and thus does not explicitly appear in the model equations.

The total precipitation in a given box is calculated as the convergence of the moisture fluxes

$$P - E = -\nabla \cdot (F_{Mq} + F_q) \tag{16}$$

This total precipitation is spread evenly over the box area. We then calculate the fraction falling on the land ice and sea ice (based on the relative areas covered by land ice and sea ice). The precipitation falling on the land and sea ice is assumed to turn into additional land and sea ice, respectively. Finally, the residue part of the total precipitation (namely, the precipitation on the open ocean and the precipitation over bare land which reaches the ocean by river runoff) is added to the freshwater forcing for the ocean model.

2.3. Land Ice Model

The land ice sheet model (Figure 2) assumes a simple two-dimensional ice sheet, neglecting variations in the zonal direction [*Weertman*, 1976; *Ghil*, 1994; *Pollard et*

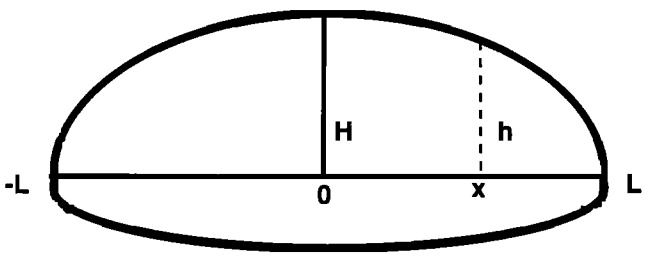

Figure 2. Land ice sheet geometry.

al., 1980]. The ice dynamic is approximated as perfect plasticity, so that the ice sheet thickness, h, is parabolic in latitude, $(h/H)^2 = 1 - y/L$. Bedrock deflection under the load of the ice is assumed instantaneous [*Weertman*, 1976; *Källén et al.*, 1979; *Ghil and Le Treut*, 1981; *Peltier*, 1994], and is given by the density ratio of the ice and that of the Earth's upper strata, resulting in 2/3 of the thickness of the ice sheet being above mean sea level (the absolute height does not affect the dynamics, as we neglect the elevation-desert effect [*Sakai and Peltier*, 1997]). The ice sheet mass balance equation is

$$\frac{dV_{\text{ice-sheet}}}{dt} = LI_{\text{Source}} - LI_{\text{Sink}}. \quad (17)$$

The source (accumulation) term, LI_{Source}, is based on the amount of precipitation in the polar boxes, assumed to be distributed evenly in the box. We assume that the precipitation falling on the ice sheet in the polar boxes turns into additional ice and supplements the source term for the glaciers there (it is implicitly assumed that the temperature is sufficiently cold for the precipitation to accumulate as new ice). Furthermore, we assume that close enough to the poles, even when there is no glacier, the precipitation still is accumulated to form new ice and supplement the glacier source term. More specifically, it is assumed that precipitation falling on the poleward 0.25 area of the polar boxes is accumulated as new ice even when no ice already exists there. Thus our accumulation term is

$$LI_{\text{Source}} = \frac{\max\{0.25\,L_{\text{area}},\, LI_{\text{area}}\}}{box_{\text{area}}}(P - E), \quad (18)$$

in which LI_{Source} is the amount of precipitation that turns into land ice, L_{area} is the land area in the box, LI_{area} is the ice sheet area, and box_{area} is the total area of the box. The $0.25\,L_{\text{area}}$ factor represents the above assumption regarding the building of new land ice, and the model is not sensitive to the exact value of this parameter (0.20 or 0.30 will produce similar results).

The ice sheet can decrease as a result of ablation which includes melting followed by ice runoff, evaporation, and calving processes [*Paterson*, 1994], all represented by LI_{Sink} in (17). We assume that the sum of these processes is constant in time, as we expect the source term dependence on the temperature to dominate that of the sink term [*Källén et al.*, 1979; *Ghil et al.*, 1987]. Temperature-dependent melting due to dust loading [*Peltier and Marshall*, 1995] or due to enhanced ice sheet collapse [*Watts and Hayder*, 1984] during deglaciation was previously used in order to obtain abrupt glacial terminations. As will be seen below, our model produces these abrupt terminations with a constant LI_{Sink} term, due to the sea ice feedback. As was noted above, land ice ablation affects the ocean salinity through $Q_S^{\text{land-ice}}$ in (5). In order for the ice sheet to grow, there should be excess of accumulation over ablation whether the ablation is constant or variable. We choose the simplest assumption (of constant ablation) that allows us to investigate the sea ice switch mechanism. More complex models of the ice sheet mass balance [*Huybrechts and Oerlemans*, 1990; *Huybrechts et al.*, 1991] also indicate that in the glacial-interglacial states of the climate system the assumption of constant ablation is fairly reasonable as a first approximation. In addition, while investigating the role of orbital forcing [*Gildor and Tziperman*, 2000] we have allowed the ablation to be a function of the summer insolation, and the oscillation mechanism has not been affected much (although its shape has become more realistic).

We calculate the meridional extension of the ice sheet on the basis of the parabolic geometry which is a result of the assumed ice sheet dynamics discussed above [*Weertman*, 1976; *Pollard et al.*, 1980; *Ghil*, 1994] and the calculated ice volume. In the northern box, the glaciers never cover the full land area as glacier growth is limited by the sea ice switch mechanism.

Observed changes in land ice sheet cover between glacial and interglacial periods occurred mostly in the Northern Hemisphere [*Crowley and North*, 1991], while Antarctica seemed to have always been fully ice covered. Therefore the land ice in the southern box is constrained in the model to cover an area equal to Antarctica, and is kept constant during the model run.

3. Results

We have run the coupled ocean-atmosphere-sea ice-land ice model and have obtained interesting variability on a timescale of 100 kyr. In this section we describe and analyze the results and, in particular, the crucial role played by the sea ice.

3.1. Analysis of the 100-kyr Cycle Mechanism

The temporal evolution of northern land ice extension during 1000 kyr is presented in Figure 3. The evolution of some key model variables during our "standard" run, using the parameters specified in the above section and in Table 1, is shown in Figure 4. Consider now the full oscillation between years 170,000 and 70,000 in Figure 4 (time is in "before present" model years, although no correspondence to actual time before present is meant; such correspondence is relevant only when Milankovitch forcing is included [*Gildor and Tziperman*, 2000]). Initially, the ocean is ice free (Figure 4b) and the atmospheric temperature (Figure 4c)

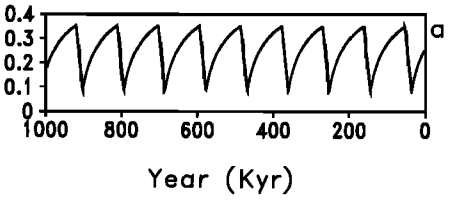

Figure 3. Land ice extent in the northern polar box as a fraction of land area in the control run.

and oceanic temperatures (Figure 4g) in the northern box are rather mild. The amount of precipitation enabling glacier growth in the northern polar box exceeds the melting and calving terms (Figure 4f, year 170,000), and therefore the glacier gradually grows (the northern box atmospheric temperature (Figure 4c), while relatively mild, is still below freezing, enabling the glacier to grow). The spreading of the land glacier increases the albedo, and consequently the temperature of the atmosphere and of the ocean in the corresponding polar box decreases slowly with the growing glaciers (Figures 4c and 4g). Eventually, around year 90,000, the sea surface temperature (SST) reaches the critical freezing temperature, $T^{\text{sea-ice}}$, and sea ice (Figure 4b) starts to form very rapidly. The creation of sea ice further increases the albedo, further reduces the atmospheric temperature, and enhances the creation of more sea ice. The characteristic timescale of sea ice growth is very short, and in less than 20 years nearly the entire polar box ocean surface is covered by sea ice. The sea ice "switch" is now turned to "on." The sea ice growth is self-limiting: the sea ice grows when the ocean temperature is cooled by the air-sea heat flux to below the freezing temperature (see equation (8)). When the sea ice cover increases, it insulates the ocean from the colder atmosphere and reduces the oceanic heat loss. The oceanic advection and diffusion of heat from the midlatitudes then balances the reduced cooling by the atmosphere, resulting in no more net cooling of the ocean and no more sea ice growth.

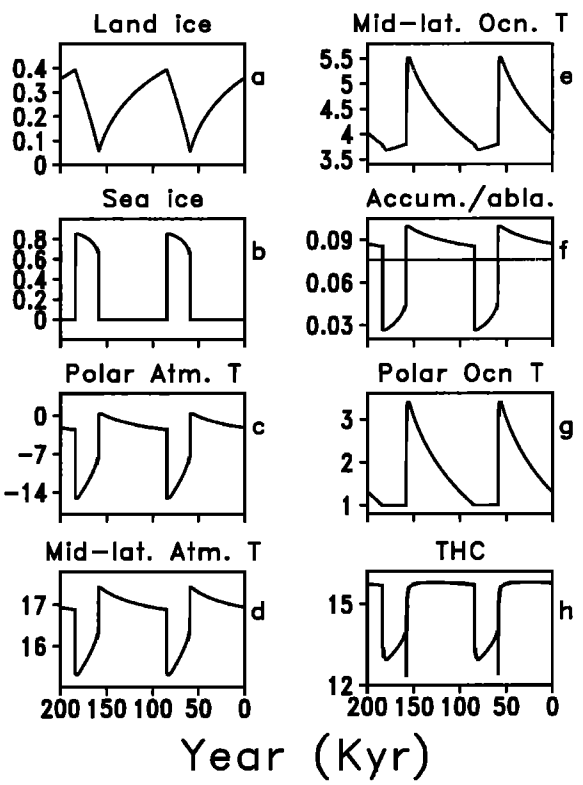

Figure 4. Model result time series for 200 kyr showing (a) northern land ice extent as a fraction of the polar land box area, (b) northern sea ice extent as a fraction of polar ocean box area, (c) northern atmospheric temperature ($°C$), (d) midlatitude atmospheric temperature ($°C$), (e) temperature in the northern midlatitude deep oceanic box ($°C$), (f) source term (solid line) and sink term (dashed line), for northern land glacier ($10^6\, m^3\, s^{-1}$), (g) temperature in the northern upper polar oceanic box ($°C$), and (h) thermohaline circulation through the northern polar boxes ($10^6\, m^3\, s^{-1}$).

When the sea ice reaches its maximal extent, the atmospheric temperature is at its minimum point. At this stage, the average global temperature is lowest, sea ice and land ice sheet extents are maximal, and the system is at a glacial maximum. Because of the low atmospheric temperature, there is a large decline in poleward moisture flux. Similarly, the extensive sea ice cover limits the evaporation from the polar ocean and further reduces the moisture supply to the land glaciers. The amount of precipitation contributing to the formation of land ice is therefore reduced to about half of its maximum value. As ablation proceeds as before, being less sensitive to temperature than precipitation, the glaciers start retreating. As the glaciers waste away, their total albedo decreases, the atmospheric temperature starts to rise slowly, and with it ,the oceanic temperature rises. As long as sea ice is present, however, there is not enough precipitation to overcome the land ice sink terms, and the glacier thus reduces fairly rapidly. The climate system is now in the termination stage of the glacial period, moving into the interglacial.

Once in the termination phase, and with land ice starting to melt, the global temperature starts increasing. This decreases the cooling of the polar ocean and thus starts a slow melting of the sea ice due to the heat advected and diffused by the ocean from midlatitudes. As long as sea ice exists, the oceanic temperature in the polar box cannot rise above the freezing temperature. The melting of the sea ice is initially fairly gradual (Figure 4b, years 90-70 kyr), until the deep ocean is sufficiently warmed (Figure 4e, years 70 kyr); then the sea ice melting becomes very rapid, and within 40 years the ocean is free of sea ice. The deep ocean warms during this phase because it is affected by vertical mixing from the upper ocean that is, in turn, affected by the global warming due to the melting of land ice. Note that the deep ocean therefore plays an important role in providing a delay time affecting the sea ice extent. The sea ice switch is now turned to "off." The lack of the land ice and sea ice increases significantly the temperature of both the atmosphere and the ocean and with it the amount of precipitation available for land ice growth. By the time the sea ice reaches its minimal extent, so does the land ice. The cycle in the glacier volume is equivalent to about 100 m of sea level change. At the end of the sea ice melting, the average temperature is at its maximum point, the ice sheet is at its minimal extent, and the ocean is free of sea ice. The cycle reaches its starting point again,

where precipitation on the glacier exceeds melting and the glacier is in a growth period. The amplitude of global temperature changes in our model is about 3° in the atmosphere and 1° in the globally averaged ocean SST, not far from the Climate: Long Range Investigation, mapping, and Prediction (CLIMAP) estimate for the ocean (1.6° in the global ocean SST [*Crowley and North*, 1991]). Note that our "SST" represents the upper 400 m of the ocean, and hence a smaller cooling is to be expected for this model temperature than the observed SST cooling. In any case, while several of the characteristics of the model glacial cycles do not match observed features, our take home message from this model is not the detailed structure of the above cycle, but the possible role played by the sea ice as a climate switch.

The thermohaline circulation is often conjectured to play a major role in creating climate transitions or transferring climatic signal between different regions and different components of the climate system [*Broecker and Denton*, 1989]. The THC flowing through the northern polar box in our model is shown in Figure 4h. At the beginning of the interglacial period, immediately after the land glaciers reach their minimal extent and all the sea ice melts, the polar salinity is low and the ocean temperature is high. At this stage the THC is at a minimum, especially owing to the freshwater pulse associated with the sea ice melting, and is at about 12 Sv. The THC recovers fairly quickly once the freshwater pulse is mixed within the entire ocean and intensifies to about 16 Sv. From that point, the THC is relatively constant until sea ice starts to form, when the THC weakens to about 13 Sv. Paleo-observations indicate that the THC was at its weakest point during the peak of the last glacial period [*Boyle and Keigwin*, 1987]. It is believed that less evaporation because of the lower temperature during glacial times decreased the surface salinity and enhanced intermediate water formation at the expense of deep water formation. In our model, this effect is not very strong, since the reduced evaporation is offset by reduced precipitation and by the brine rejection effect due to sea ice formation. The model THC is weaker during the coldest period which extends from the peak glacial into the deglaciation period, which is consistent with the paleo-observations. However, we will see below that the THC variability is not essential to the glacial-interglacial oscillation in our model (section 4.4). In fact, the thermohaline circulation changes and instabilities in our model are not the trigger of rapid climate changes [*Broecker et al.*, 1985; *Rahmstorf*, 1995; *Tziperman*, 1997] but, rather, are a result of the rapid sea ice switches (it is still possible, of course, that in reality, or even in a different variant of our box model, the THC could play a larger role than that in our present model simulations).

Rapid climate changes that occurred within a few decades have been seen in several climate proxies [*Taylor et al.*, 1993; *Alley et al.*, 1993; *Lehman and Keigwin*, 1992]. In our model, a full retreat of land ice sheets occurs on a timescale of several thousands years but changes in the extent of sea ice, and the resulting changes in atmospheric temperature, in the THC, and in the rate of accumulation over glaciers are very rapid and last only a few decades. The sea ice "switch" may therefore account not only for the glacial-interglacial transitions on a 100-kyr timescale but perhaps also for the many rapid climate transitions seen in the proxy observations in the context of shorter-term variability.

The eight ocean boxes and four atmospheric boxes present a significantly increased resolution from that used in previous simple models of the glacial-interglacial transitions [e.g., *Saltzman and Verbitsky*, 1993; *Paillard*, 1998]. Still, one wonders whether the rapid sea ice switches may be an artifact of the use of a single box temperature for the entire upper Northern Hemisphere polar ocean. In the actual climate system, sea surface temperature varies gradually with latitude, and one might expect the sea ice cover to slowly grow or retreat as this SST gradient changes slowly in time in response to changing land glaciers. The extensive seasonal changes of sea ice cover in the present-day northern ocean and during the last glacial maximum [*Weinelt et al.*, 1996], as well as some previous modeling studies [*Thorndike*, 1992], support the feasibility of rapid sea ice changes that we find to last a few tens of years. Note that it is only the upper ocean that needs to cool rapidly to enable the switch behavior, and such an upper ocean temperature adjustment is indeed expected to take tens of years in the real ocean. The deep ocean still plays an important role, as explained above, in providing a delayed response due to its large heat capacity.

The present model is forced with annual mean radiation, neglecting seasonal and orbital forcing. These effects are included in the study presented in a subsequent paper [*Gildor and Tziperman*, 2000]. The mechanism discussed here is shown in that paper to be independent of the seasonal cycle and orbital forcing. Specifically, it is shown that the reduced sunlight during the winter season when the sea ice cover is maximal does not inactivate the sea ice switch behavior. Similarly, it is shown that a seasonal sea ice cover is sufficient to affect the moisture source for the land glaciers. The orbital forcing is shown to be important in pacing the glacial oscillations and phase locking them to the Milankovitch variations in solar radiations, as was seen in previous studies using different glacial oscillation mechanisms [*Saltzman*, 1990; *Paillard*, 1998].

3.2. Why the 100-kyr Timescale?

The glacial oscillation in our model is a nonlinear relaxation oscillation. Based on the insight we have obtained into the oscillation mechanism, we can now formulate a simple argument for the 100-kyr timescale. Let the variable part of the land glaciers have a volume $\Delta V = V_{\max} - V_{\min}$. Assume that the glacier

is fed at either a maximum accumulation rate $M_{\max}$ (during an interglacial period) or at a minimum rate $M_{\min}$. This is not a bad approximation to the shaper of the source term shown in Figure 4f, solid line. Let the sink term due to ablation be represented by a constant S. The glacier grows from $V_{\min}$ to $V_{\max}$ in a time $\Delta V/(M_{\max} - S)$. Once reaching $V_{\max}$, the sea ice grows and switches the system to the minimum accumulation rate $M_{\min}$, and the glacier retreats back to $V_{\min}$ within $\Delta V/(S - M_{\min})$. A full cycle therefore lasts $\tau = \Delta V[(M_{\max} - S)^{-1} + (S - M_{\min})^{-1}]$. Now $V_{\max}$ and $V_{\min}$ are determined by the land ice albedo values required to turn the sea ice switch on and off, while the accumulation rates $M_{\min}$ and $M_{\max}$ are determined by the atmospheric dynamics. The timescale τ as a function of the sink S has a minimum at $S = (M_{\min} + M_{\max})/2$ (where the oscillation is symmetric and has equal lengths of the growing and retreating glacier periods). With order-of-magnitude values of $\Delta V = 2.4\,10^{16}\ m^3$, $M_{\max} = 0.09\,10^6\ m^3/s$, $M_{\min} = 0.03\,10^6\ m^3/s$, one obtains $\tau_{\min} = 50$ kyr. For an asymmetric oscillation where the glacier fills during 85% of the period and retreats during the remaining 15%, one finds $S = 0.081\,10^6\ m^3/s$ and $\tau = 100$ kyr. A straightforward linear estimate based on the time it would take the precipitation to fill up the land glacier gives a far less realistic $\tau_{\text{linear}} = \Delta V/M_{\max} = 10$ kyr.

4. Parameter Sensitivity

The study of the model's sensitivity to some of its key parameters may shed additional light on the climate variability mechanism, and we therefore describe now several sensitivity experiments, devoting a subsection to each parameter. We will see that the insight gained from the sensitivity experiments is consistent with the simple argument given in subsection 3.2 for the source of the 100-kyr timescale. Table 2 summarizes the sensitivity experiments, their parameter choices, and the relevant subsection and figure numbers.

4.1. Land Ice Sink Term

This term (LI_{Sink} in equation (17)) represents processes such as glacier melting, calving, and runoff. When the LI_{Sink} term in the Northern Hemisphere is reduced by about 4% (experiment SINK1, Table 2), the timescale of the oscillation becomes shorter by about 10 kyr relative to the control run (Figure 5a). The reduced sink term allows the glacier to reach faster the critical size at which the glacier albedo reduces the temperature sufficiently to allow the sea ice to start growing. Similarly, the deglaciation phase takes longer when the sink term that drives the deglaciation is reduced. Consequently, the shape of the oscillation becomes less sawtooth like and more symmetric, consistent with the simple timescale argument given in section 3.2. Similarly, when LI_{Sink} is increased by 4%, the oscillation timescale increases by about 16 kyr (Figure 5b). This is again consistent with section 3.2 which predicts a very long timescale as the sink approaches the maximum source value ($S \longrightarrow M_{\max}$). Increasing this term even more, by about 20%, makes the sink term always exceed the precipitation and formation of new ice, and the glacier eventually disappears. When reducing the sink term by a significant amount, say 45%, the longer timescale of glacier sink term enables the system to adjust into a nonoscillatory steady state. The LI_{Source} term then equals the LI_{Sink} term, the sea ice covers about half of the oceanic box and the land ice covers about 10% of the land area. Overall, the sensitivity to this parameter is not negligible, yet it cannot be used to reduce the model timescale for the glacial-interglacial cycle to significantly less than 100 kyr, and the sensitivity is also completely consistent with the scaling argument of section 3.2.

4.2. Albedo

In experiments ALBEDO1 and ALBEDO2, the albedo of the land ice and of the sea ice was varied by 0.05 (i.e., by about 6-7%). A reduction in both albedos causes an increase in the oscillation timescale, as can

Table 2. Parameters Changed in the Sensitivity Experiments

Experiment Name	Parameters Changed	Standard Value	New Value	Section/Figure
SINK1	$LI_{\text{Sink},4}$	0.076	0.073	4.1/5a
SINK2	$LI_{\text{Sink},4}$	0.076	0.079	4.1/5b
ALBEDO1	$\alpha_{\text{land-ice}}$, $\alpha_{\text{sea-ice}}$	0.85, 0.65	0.80, 0.60	4.2/6a
ALBEDO2	$\alpha_{\text{land-ice}}$, $\alpha_{\text{sea-ice}}$	0.85, 0.65	0.90, 0.70	4.2/6b
EMISSIVITY1	$P_{lw1}, \cdot\cdot, P_{lw4}$	0.58, 0.56, 0.54, 0.626	0.577, 0.557, 0.537, 0.623	4.3/7a
EMISSIVITY2	$P_{lw1}, \cdot\cdot, P_{lw4}$	0.58, 0.56, 0.54, 0.626	0.583, 0.563, 0.543, 0.629	4.3/7a
THC-MEAN	THC's strength	free to change	fixed at mean value	4.4/8
T freeze up	$T^{\text{sea-ice}}$	274 °K	274.5 °K	4.6/-
T freeze down	$T^{\text{sea-ice}}$	274 °K	273.5 °K	4.6/-
Ice thickness up	$D_{\text{sea-ice}}$	2 m	3 m	4.5/-
Ice thickness down	$D_{\text{sea-ice}}$	2 m	1 m	4.5/-
Atm merid heat	F_{merid}	free to evolve	constant	4.7/9

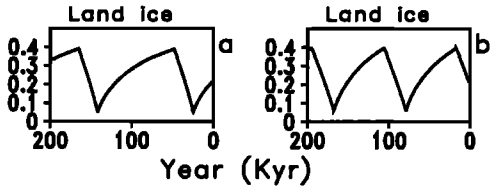

Figure 5. Time series of land ice extent as a fraction of the northern land box area in the experiments examining the sensitivity to the glacier sink term LI_{Sink}: (a) 4% reduction in LI_{Sink} and (b) 4% increase in LI_{Sink}.

be seen in experiment ALBEDO1 (Figure 6a), where a full cycle requires 112 kyr compared with 100 kyr in the standard run. A reduced albedo requires that the land ice becomes larger in order to achieve the same total albedo effect. This takes more time, hence the longer cycle. Similarly, increasing both albedos simultaneously (ALBEDO2) shortens the timescale to 87 kyr (Figure 6b). Less land ice is needed in this case in order for the land ice albedo to reduce the ocean temperature below the critical freezing temperature. On the other hand, during the land ice retreat stage of the glacial cycle, the glacier should also become smaller than before to enable a temperature increase that results in the melting of the sea ice. Thus the increased albedo shortens the glacier growth phase and lengthens the retreat phase. The total effect is a shorter timescale of the entire cycle and a more symmetric cycle.

Increasing the sea ice albedo in our model by a significantly larger amount causes the climate system to go into a state of permanent sea ice cover and no land ice cover. Decreasing the sea ice albedo significantly will make it less effective as a climate switch and eventually eliminate the climate switch mechanism. Increasing the land ice albedo up to 100% just reduces the amplitude of the oscillation and shortens the timescale, while decreasing it by a significant amount increases significantly the timescale needed to turn on the sea ice switch. When it is too low, the sea ice switch is not turned on even when the whole polar box is covered by land ice.

4.3. Emissivity

The longwave emissivity coefficient in the atmospheric model, P_{lw}, represents factors such as cloud cover, humidity, and atmospheric concentration of aerosols and CO_2 and is different for each atmospheric box. If we assume that the emissivity is composed of a constant part which does not depend on CO_2 concentrations, P^*_{lw}, and a part which includes the CO_2 effect alone, P'_{lw}, then we can write $P'_{lw} = 0.015 * \ln[CO_2/CO_{2ref}]$ [*Peltier and Marshall*, 1995]. This results in a radiative forcing of approximately 4 W/m^2 for a CO_2 doubling. A 30% change in CO_2 concentration, as occurred on a glacial-interglacial timescale [*Bender et al.*, 1997], is thus equivalent to changing P_{lw} by about 0.003.

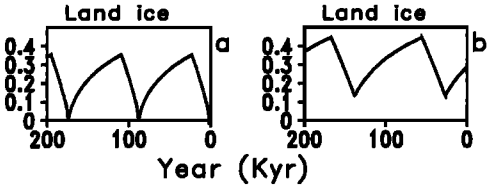

Figure 6. Land ice extent as a fraction of the northern land box area in sensitivity experiments to (a) reduction and (b) increase of the albedo of both land ice and sea ice by 0.05.

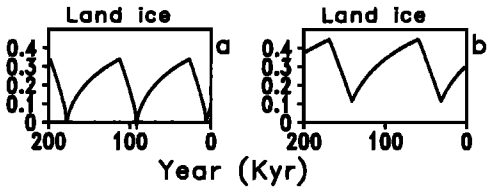

Figure 7. Land ice extent as a fraction of the northern land box area in sensitivity experiments to (a) reduction and (b) increase of the emissivity by 0.003.

A reduction of the emissivity by 0.003 does not change the model results qualitatively but only increases the timescale by about 9 kyr (experiment EMISSIVITY1, Figure 7a). As a reduction of this term is equivalent to higher CO_2 intense greenhouse effect, it makes the whole climate system warmer; so larger glaciers and longer periods are required for the SST to reach the freezing threshold. Increasing the emissivity by 0.003 cools the climate, and as a result, the timescale is now shorter by about 12 kyr (Figure 7b).

Reducing the emissivity even more causes a farther increase in the timescale. Increasing the emissivity by more than 0.005 cools the climate to such a degree that the sea ice cover becomes permanent and the model's glacial-interglacial cycle does not exist.

4.4. Thermohaline Circulation

Changes in the strength of the THC, especially in the North Atlantic, are known to be correlated with climatic changes [*Lehman and Keigwin*, 1992; *Jansen and Veum*, 1990; *Boyle and Keigwin*, 1987]. This seems to have led to a consensus that the changes in the THC are what caused the climate transitions. This motivates the experiment THC-MEAN in which the strength of the THC between each pair of ocean boxes in experiment THC-MEAN is set to be constant in time and equal to its mean value in the standard run. The temperature and salinity in the ocean still vary, but the resulting density variations do not affect the strength of the THC.

Figure 8 shows the land ice extension (Figures 8a and 8d), the amount of heat transfered to the atmosphere by the ocean in the northern polar box (Figures 8b and e), and the THC through the northern polar box (Figures 8c and g) from the standard (Figures 8a, 8b, 8c) and from experiment THC-MEAN (Figures 8d, 8e, 8f). The glacial-interglacial oscillation still exists with the "frozen" THC and is qualitatively similar to

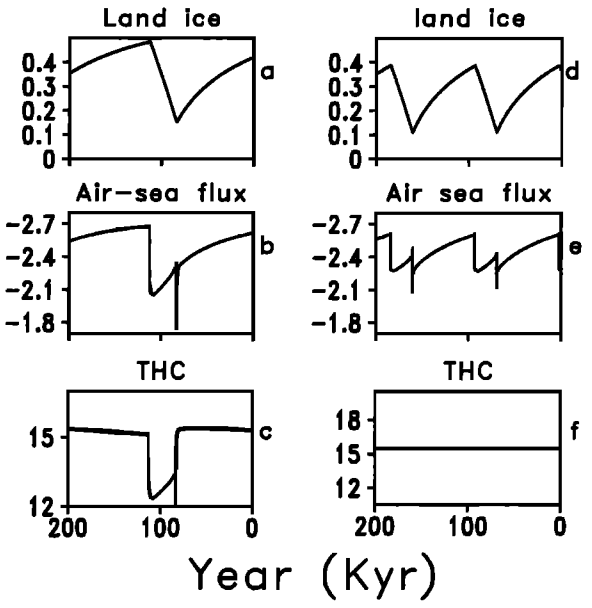

Figure 8. Model results (a,b,c) in the control experiment and (d,e,f) when setting the strength of the THC to a constant in time. (a,d) Land ice extent as a fraction of the northern land box area. (b,e) Heat transferred to the atmosphere from the northern polar oceanic box. (c,f) THC through the northern polar oceanic box (Sv).

its shape in the control run. This seems to indicate that the THC variability is not an essential component of the glacial-interglacial oscillation mechanism in our model. Given that the THC variability in the control run is small (Figure 4h), it is not surprising, perhaps, that the glacial cycle is not strongly affected by freezing the amplitude of the THC in our model. However, the glacial-interglacial oscillations mechanism analyzed above clearly does not depends on THC feedback. We therefore propose that the THC is not necessarily a crucial component of the glacial dynamics, but perhaps only responds to and somehow amplifies the variability of other climate components.

There are quantitative changes to the glacial cycle in experiment THC-MEAN. The timescale of the oscillation in this experiment is a bit shorter for two reasons. First, near the initial sea ice growth stage, when the THC is weaker than that in the standard run, less heat is transported to the polar ocean box. The colder polar box therefore requires a bit less of the land ice albedo effect to cross the threshold for initiating sea ice growth (the slightly reduced maximal extension of land ice can be seen in Figure 8a compared with Figure 8d). Second, during the stage of rapid melting of sea ice, at the final stage of the deglaciation, the THC is stronger than that in the standard run, bringing more heat and accelerating the melting. The combined effect is to shorten by a few kiloyears the time of a full glacial-interglacial oscillation.

As was noted above, the oceanic meridional heat transport carried by the THC in the model is 2.3 PW in the standard run. Glacial oscillations are seen to exist in the model, however, for a wide range of such transport, up to 3.3 PW, again demonstrating the robustness of the oscillation mechanism.

4.5. Ice Thickness

We have tested the sensitivity of the model to the specified sea ice thickness. While in the standard case the sea ice formed in the northern polar box has a uniform thickness of 2 m, we ran the model also with thicknesses of 1 m and 3 m (runs "ice thickness down" and "ice thickness up" in Table 2). There are only very minor differences between these experiments. This is not surprising, as the sea ice influences the climate system mainly through its albedo and its insulating effect. The insulating effect depends very weakly on the ice thickness, and the albedo effect is determined by the area covered by sea ice.

4.6. Freezing Temperature

As sea ice plays a most important role in the suggested mechanism, we have conducted sensitivity experiments to another parameter of the sea ice model, the critical temperature of freezing. We conducted two experiments, raising and lowering the critical temperature by 0.5° ("T freeze up" and "T freeze down" in Table 2). In both cases, similar glacial-interglacial oscillations still exist: when lowering the freezing temperature, the timescale becomes longer by about 20 kyr; when increasing the freezing temperature, the timescale becomes shorter by about 20 kyr. The mechanism responsible for these changes is similar to that discussed in section 4.3.

4.7. Atmospheric Meridional Heat Transport

Meridional heat transport is expected to be crucial in the suggested mechanism, as it affects the northern box temperature and hence the amount of precipitation available for glacier growth. We have therefore ran the model with two other types of meridional heat transport parameterizations: Stone's type parameterization [*Stone*, 1972] and constant meridional transport of heat (run "atm merid heat" in Table 2). The model glacial oscillation exists with minor differences with these two types of meridional heat transport parameterizations. Figure 9 compares the constant meridional heat transport case with the standard run, in which there are significant differences in the meridional heat transport between glacial and interglacial periods. Nevertheless, as can be seen, the results in both cases are quite similar.

5. Conclusion

We have used a simple zonally averaged coupled atmosphere, ocean, land ice, and sea ice box model to demonstrate a novel mechanism for the glacial-interglacial cycles, with some of the main observed character-

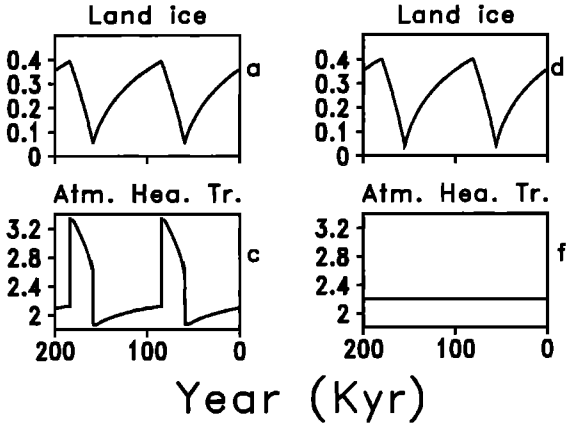

Figure 9. Model results (a,b) in the control experiment and (c,d) when setting the strength of the atmospheric meridional heat transport to a constant in time. (a,c) Land ice extent as a fraction of the northern land box area. (b,d) Meridional heat transport (PW).

istics such as the the 100-kyr timescale and the asymmetric sawtooth shape. Both of these features are fairly robust: the timescale of the oscillation has not deviated from 100 kyr by more than 30% for reasonable parameter choices, and the asymmetric sawtooth structure is inherent to our oscillation mechanism (being a relaxation oscillation mechanism). We were also able to formulate a simple explanation for the 100-kyr timescale, based on the analysis of the glacial cycle mechanism in our model. The glacial-interglacial oscillations in our model result from a combination of the temperature-precipitation and temperature-albedo feedbacks [*Källén et al.*, 1979]. However, both the timescale and the asymmetric sawtooth structure are determined in our model by a novel sea ice feedback in which the sea ice grows and melts within a few decades and acts as a switch of the climate system, switching it between growing and retreating land ice modes. The large albedo effect of a significant sea ice cover dramatically reduces the atmospheric temperature, the atmospheric humidity available for precipitation, and the local evaporation from the polar ocean. These combine to also reduce the atmospheric precipitation over the land glaciers. The land glaciers, lacking the moisture source for their growth, start to retreat relatively rapidly owing to ablation. The sea ice switch plays a similar role in switching the system back to a growing land ice mode. As the land glaciers shrink, the atmospheric temperature increases slowly through the land ice albedo feedback, until the sea ice switch is turned to off, i.e., no sea ice. The disappearing of sea ice causes the atmospheric temperature to increase, and as a result the meridional atmospheric transport of moisture increases as well. Similarly, without the insulating sea ice cover, the extraction of moisture from the polar ocean increases, and together with the increased meridional moisture flux, this provides a stronger rate of precipitation over the land glaciers, which can now grow again.

The switch-like behavior of sea ice in our model is consistent with its well-known rapid response time to changes in the climate system, even on a seasonal timescale. Other model results [*Thorndike*, 1992] also support the idea that reasonable changes in the heat budget of the northern ocean can cause dramatic changes in the sea ice cover. Sea ice impact on the availability of atmospheric moisture sources for ice sheet growth was already recognized in early studies [*Stokes*, 1955; *Ruddiman and McIntyre*, 1981], and so was its crucial effect on the Earth's albedo. Rapid climate changes abound in the proxy record, and one wonders if the rapid and drastic response of the sea ice to atmospheric and oceanic temperature changes might provide a natural and simple explanation for these observed climate switches, in addition to the role we are proposing for it in shaping the 100-kyr glacial cycle.

An important aspect of our model solution is the occurrence of land ice deglaciation in phase with extensive sea ice cover and hence a relatively cold period. Presently available sea ice proxy data [*de Vernal and Hillaire-Marcel*, 2000; *de Vernal and Pedersen*, 1997] still lack the spatial and temporal resolution which would enable us to resolve the sea ice phase relative to that of the major deglaciation. Nevertheless, they seem to indicate that extensive sea ice cover has existed for a few kiloyears after the last glacial maximum. Melt water pulses due to deglaciation were believed for some time to have occurred during the Bølling/Allerød and Preboreal warm periods [*Fairbanks*, 1989]. This was challenged by more recent studies [*Bard et al.*, 1996] which showed evidence for one rather than two pulses, showed that a more constant rate of deglaciation fits the data well, and placed the melt water pulse within a cold event that followed the initiation of the Bølling/Allerød warm period. In addition, note that the temperature effect of the sea ice switch is mostly in the atmospheric temperature, while the high-latitude ocean temperature reflected in ocean sediment proxies is already cold during all phases of the glacial cycle and is not expected to vary very dramatically owing to the presence of sea ice. Isotopic composition of precipitation over land, which is used in ice core proxy measurements of atmospheric temperature, may be influenced by the source of the precipitation, and this source can vary very dramatically owing to the effects of sea ice on the atmospheric circulation [*Charles et al.*, 1994]. Given these uncertainties and especially given the lack of a satisfactory detailed physical mechanism for the glacial cycles (as opposed to just a fit to the available proxies), we argue that it would be useful to keep an open mind regarding a possible sea ice control of glacial dynamics, while examining both the available proxy record and new proxy data that become available. Because of the difficulties in correlating climate proxies from different sources, what is needed are proxies from which information on the relative timing of sea ice and land ice can be extracted.

The glacial cycles are purely periodic in our model as long as the processes described above are the only ones to operate. In reality, Milankovitch forcing introduces some additional variability [*Gildor and Tziperman*, 2000], volcanic eruptions may affect the radiation balance and hence the temperature, the isostatic adjustment neglected here may introduce additional shorter timescales, instabilities in the glaciers may (a)periodically discharge large icebergs, and the system's nonlinearity may lead to a chaotic behavior even without such external stochastic factors [*Ghil*, 1994].

The purpose of the present model, being highly idealized, is to explore a limited set of feedbacks rather than produce a realistic simulation of the glacial cycles. The model fails to reproduce, for example, the synchronous deglaciation of the Southern Hemisphere. There are almost no changes in sea ice cover in the southern polar box during the cycles. A more explicit representation of the Southern Ocean dynamics which takes into account the wind-driven upwelling, for example, is needed. The lack of Southern Hemisphere changes could also be due to the lack of CO_2 feedback which could transmit information between the hemispheres [*Genthon et al.*, 1987] or due to the lack of an explicit sea level glacier instability mechanism which could be especially important for the Antarctica ice sheet [*Paterson*, 1994; *Huybrechts and Oerlemans*, 1990]. It should be noted that the glacial oscillation analyzed above exists within a certain parameter regime which, although not small, is still finite. Outside this regime, various steady states of the climate system can be found in the model (characterized by constant land glacier extent, or by no land glaciers, or no sea ice, or possibly by an ice-covered Earth, etc). The model behavior in the investigated parameter regime seems to be relevant to the observed glacial cycles and, we hope, helps elucidate the role of sea ice in these cycles.

In spite of these obvious shortcomings of our idealized model simulation, we feel this model has captured some potentially important and interesting feedback of the sea ice role in the glacial-interglacial cycles. In a subsequent paper we explore the role of Milankovitch forcing in the glacial-interglacial oscillation mechanism analyzed here [*Gildor and Tziperman*, 2000]. We plan to approach the role of the ocean geochemistry and variable greenhouse gases at the next stage.

Acknowledgments. We thank Michael Ghil, Aldo Shemesh, Isaac Held, and Robbie Toggweiler for numerous useful discussions. We thank Ilya Rivin and Eyal Heifetz for their advice on the atmospheric model parameterizations and Mike Winton and Vladimir Katssov for discussions regarding the sea ice model. We thank Mark Cane and two anonymous reviewers for their detailed and constructive comments that greatly improved the presentation. This work is partially supported by the Israeli-U.S. Binational Science Foundation.

References

Alley, R. B., et al., Abrupt increase in Greenland snow accumulation at the end of the Younger Dryas event, *Nature, 362*, 527–529, 1993.

Bard, E., B. Hamelin, M. Arnold, L. Montaggioni, G. Cabioch, G. Faure, and F. Rougerie, Deglagical sea level record from Tahiti corals and the timing of global meltwater discharge, *Nature, 382*, 241–244, 1996.

Bender, M., T. Sowers, and E. Brook, Gases in ice cores, *Proc. Natl. Acad. Sci., U. S. A., 94*, 8343-8349, 1997.

Birchfield, E. G., J. Weertman, and A. T. Lunde, A model study of the role of high-latitude topography in the climatic response to orbital insolation anomalies, *J. Atmo. Sci., 39*, 71-87, 1982.

Birchfield, E. G., H. Wank, and J. J. Rich, Century/millennium internal oscillations in an ocean-atmosphere-continental ice sheet model, *J. Geophys. Res., 99*, 12,459-12,470, 1994.

Boyle, E. A., and L. Keigwin, North Atlantic thermohaline circulation during the past 20,000 years linked to high-latitude surface temperature, *Nature, 330*, 35-40, 1987.

Broecker, W. S., and G. H. Denton, The role of ocean-atmosphere reorganizations in glacial cycles, *Geochim. Cosmochim. Acta, 53*, 2465-2501, 1989.

Broecker, W. S., D. Peteet, and D. Rind, Does the ocean-atmosphere system have more than one stable mode of operation?, *Nature, 315*, 21-25, 1985.

Bush, A. B. G., and S. G. H. Philander, The role of ocean-atmosphere interactions in tropical cooling during the last glacial maximum, *Science, 279*, 1341-1344, 1998.

Charles, C. D., D. Rind, J. Jouzel, R. D. Koster, and R. G. Fairbanks, Glacial-interglacial chamges in moisture sources for Greenland: Influences on the ice core record of climate, *Science, 263*, 508-511, 1994.

Chen, D., R. Gerds, and G. Lohmann, A 1-D atmospheric energy balance model developed for ocean modeling, *Theor. Appl. Climatol., 51*, 25-38, 1995.

Crowley, T. J., and G. R. North, *Paleoclimatology*, 339 pp., Oxford Univ. Press, New York, 1991.

Cuffy, K. M., and G. D. Clow, Temperature, accumulation, and ice sheet elevation in central Greenland through the last deglacial transition, *J. Geophys. Res., 102*, 26,383–26,396, 1997.

Dansgaard, W., J. W. C. White, and S. J. Johnsen, The abrupt termination of the Younger Dryas climate event, *Nature, 339*, 532–534, 1989.

DeBlonde, G., and W. R. Peltier, Late Pleistocene ice age scenarios based on observational evidence, *J. Clim., 6*, 709-727, 1993.

de Vernal, A., and C. Hillaire-Marcel, Sea-ice cover, sea-surface salinity and halo-/thermocline structure of the northwest North Atlantic: Modern versus full glacial condition, *Quat. Res., 19*, 65-85, 2000.

de Vernal, A., and T. F. Pedersen, Micropaleontology and palynology of core PAR87A-10: A 23,000 year record of paleoenvironmental changes in the Gulf of Alaska, northeast North Pacific, *Paleoceanography, 12*, 821-830, 1997.

Donn, W. L., and M. Ewing, A theory of ice age III, *Science, 152*, 1706–1712, 1966.

Fairbanks, R. G., A 17.000 year glacio eustatic sea level record: Influence of glacial melting rates on the Younger Dryas event and deep-ocean circulation, *Nature, 342*, 637-642, 1989.

Gallée, H., J. P. Ypersele, T. Fichefet, I. Marsiat, C. Tricot and A. Berger, Simulation of the last glacial cycle by a coupled, sectorially averaged climate-ice sheet model, 2, Response to insolation and CO_2 variations, *J. Geophys. Res., 97*, 15,713-15,740, 1992.

Ganopolski, A., S. Rahmstorf, V. Petoukhov, and M. Claussen, Simulation of modern and glacial climates with a coupled global model of intermediate complexity, *Nature, 391*, 351-356, 1998.

Genthon, C., J. M. Barnola, D. Raynaud, C. Lorius, J. Jouzel, N. I. Barkov, Y. S. Korotkevich and V. M.

Kotlyakov, Vostok ice core: Climatic response to CO_2 and orbital forcing changes over the last climate cycle, *Nature, 329*, 414-418, 1987.

Ghil, M., Cryothermodynamics: The chaotic dynamics of paleoclimate, *Physica D, 77*, 130–159, 1994.

Ghil, M., and H. Le Treut, A climate model with cryodynamics and geodynamics, *J. Geophys. Res., 86*, 5262–5270, 1981.

Ghil, M., A. Mullhaupt, and P. Pestiaux, Deep water formation and Quaternary glaciations, *Clim. Dyn., 2*, 1–10, 1987.

Gildor, H., and E. Tziperman, Sea ice as the glacial cycles climate switch: Role of seasonal and Milankovitch solar forcing, *Paleoceanography, 15*, 605-615, 2000.

GRIP-Greenland-Ice-Core-Project-Members, Climate instability during the last interglacial period recorded in the GRIP ice core, *Nature, 364*, 203-207, 1993.

Hall, N. M. J., P. J. Valdes, and B. Dong, The maintenance of the last great ice sheets: A UGAMP GCM study, *J. Clim., 9*, 1004-1019, 1996.

Haltiner, G. J., and R. T. Williams, *Numerical Prediction and Dynamic Meteorology*, 477 pp., John Wiley, New York, 1980.

Haney, R. L., Surface thermal boundary condition for ocean circulation models, *J. Phys. Oceanogr., 1*, 241-248, 1971.

Hasumi, H., Ocean's role in forming the steady state of the climate, *Rep. 5*, Cent. for Clim. Syst. Res., Univ. of Tokyo, Tokyo, 1997.

Hebbeln, D., T. Dokken, E. S. Andersen, M. Hald, and A. Elverhøl, Moisture supply for northern ice-sheet growth during the last glacial maximum, *Nature, 370*, 357-360, 1994.

Huybrechts, P., and J. Oerlemans, Response of the Antarctic ice sheet to future greenhouse warming, *Clim. Dyn., 5*, 93-102, 1990.

Huybrechts, P., A. Letreguilly, and N. Reeh, The Greenland ice sheet and greenhouse warming, *Palaeogeogr., Palaeoclimatol., Palaeoecol., 89*, 399–412, 1991.

Imbrie, J., J. Hays, D. Martinson, A. McIntyre, A. Mix, J. Morley, N. Pisias, W. Prell, and N. Shackleton, The orbital theory of Pleistocene climate: Support from a revised chronology of the marine $\delta^{18}O$ record, in *Milankovitch and Climate*, part 1, edited by A. Berger et al., pp. 269–305, Kluwer Acad., Norwell, Mass., 1984.

Imbrie, J., et al., On the structure and origin of major glaciation cycles, 1, Linear responses to Milankovitch forcing, *Paleoceanography, 7*, 701–738, 1992.

Imbrie, J., et al., On the structure and origin of major glaciation cycles, 2, The 100,000–year cycle, *Paleoceanography 8*, 699–735, 1993.

Ingram, W. J., C. A. Wilson, and J. F. B. Mitchell, Modeling climate change: An assessment of sea ice and surface albedo feedbacks, *J. Geophys. Res., 94*, 8609-8622, 1989.

Jansen, E., and T. Veum, Evidence for two-step deglaciation and its impact on North Atlantic deep-water circulation, *Nature, 343*, 612-616, 1990.

Kagan, B. A., V. A. Ryabchenko, and A. S. Safray, Simulation of the seasonal evolution of the thermal regime of the ocean-atmosphere system, *Izv. Acad. Sci. USSR Atmos. Oceanic Phys.*, Engl. Transl., *20*, 34-40, 1984.

Källén, E., C. Crafoord, and M. Ghil, Free oscillations in a climate model with ice-sheet dynamics, *J. Atmos. Sci., 36*, 2292–2303, 1979.

Kapsner, W. R., R. B. Alley, C. A. Shuman, S. Anandakrishnan, and P. M. Grootes, Dominant influence of atmopsheric circulation on snow accumulation in Greenland over the past 18,000 years, *Nature, 373*, 52-54, 1995.

Kerr, R. A., Sea floor records reveal interglacial climate cycles, *Science, 279*, 1304-1305, 1998.

Krinner, G., and C. Genthon, GCM simulations of the last glacial maximum surface climate of Greenland and Antarctica, *Clim. Dyn., 14*, 741-758, 1998.

Kutzbach, J. E., and P. J. Guetter, The influence of changing orbital parameters and surface boundary conditons on climate simulations for the past 18,000 years, *J. Atmos. Sci., 43*, 1726-1759, 1986.

Ledley, T. S., and S. Chu, Global warming and the growth of ice sheets, *Clim. Dyn., 9*, 213-219, 1994.

Lehman, S. J., and L. D. Keigwin, Sudden changes in North Atlantic circulation during the last deglaciation, *Nature, 356*, 757-762, 1992.

Le Treut, H., and M. Ghil, Orbital forcing, climatic interactions, and glaciation cycles, *J. Geophys. Res., 88*, 5167–5190, 1983.

Lorius, C., L. Merlivat, J. Jouzel, and M. Pourchet, A 30,000-yr isotope climatic record from Antarctic ice, *Nature, 280*, 644-648, 1979.

Manabe, S., and A. J. Broccoli, The influence of continental ice sheets on the climate of an ice age, *J. Geophys. Res., 90*, 2167-2190, 1985.

Manabe, S., and R. J. Stouffer, Two stable equilibria of a coupled ocean atmosphere model, *J. Clim., 1*, 841-866, 1988.

Manabe, S., R. J. Stouffer, M. J. Spelman, and K. Bryan, Transient response of a coupled ocean-atmosphere model to gradual changes of atmospheric CO_2, part 1, Annual mean response, *J. Clim., 4*, 785-818, 1991.

Manabe, S., and R. F. Strickler, Thermal equilibrium of the atmosphere with a convective adjustment, *J. Atmos. Sci., 21*, 3-42, 1964.

Marotzke, T., and P. H. Stone, Atmospheric transports, the thermohaline circulation, and flux adjustments in a simple coupled model, *J. Phys. Oceanogr., 25*, 1350–1364, 1995.

Miller, G. H., and A. de Vernal, Will greenhouse warming lead to Northern Hemisphere ice-sheet growth?, *Nature, 355*, 244-246, 1992.

North, G. R., and J. A. Coakley, Differences between seasonal and mean annual energy balance model calculation of climate and climate sensitivity, *J. Atmos. Sci., 36*, 1189-1204, 1979.

Oerlemans, J., Glacial cycles and ice-sheet modeling, *Clim. Change, 4*, 353-374, 1982.

Paillard, D., The timing of Pleistocene glaciations from a simple multiple-state climate model, *Nature, 391*, 378–381, 1998.

Paterson, W. S. B., *The Physics of Glaciers*, 480 pp., Pergamon, Tarrytown, N. Y., 1994.

Peixoto, J. P., and A. H. Oort, *Physics of Climate*, 520 pp., Am. Inst. of Phys., College Park, Md., 1991.

Peltier, W. R., Ice age paleotopography, *Science, 265*, 195-201, 1994.

Peltier, W. R., and S. Marshall, Coupled energy balance/ice sheet model simulations of the glacial cycles: A possible connection between terminations and terrigenous dust, *J. Geophys. Res., 100*, 14,269-14,289, 1995.

Petit, J. R., et al., Climate and atmospheric history of the past 420,000 years from the Vostok ice core, Antarctica, *Nature, 399*, 429-436, 1999.

Pollard, D., Ice-age simulations with a calving ice-sheet model, *Quat. Res., 20*, 30-48, 1983.

Pollard, D., A. P. Ingersoll, and J. G. Lockwood, Response of a zonal climate-ice sheet model to the orbital perturbations during the Quaternary ice ages, *Tellus, 32*, 301-319, 1980.

Rahmstorf, S., Bifurcation of the Atlantic thermohaline circulation in response to changes in the hydrological cycle, *Nature, 378*, 145-149, 1995.

Raymo, M. E., Glacial puzzles, *Science, 281*, 1467–1468, 1998.

Rind, D., D. Peteet, and G. Kukla, Can Milankovitch orbital variations initiate the growth of ice sheet in a general circulation model?, *J. Geophys. Res., 94*, 12,851-12,871, 1989.

Rivin, I., and E. Tziperman, Linear versus self-sustained interdecadal thermohaline variability in a coupled box model, *J. Phys. Oceanogr., 27*, 1216–1232, 1997.

Robin, G. D. Q., Ice cores and climatic change, *Philos. Trans. R. Soc. London, Ser. B, 280*, 143-168, 1977.

Ruddiman, W. F., and A. McIntyre, Oceanic mechanisms for amplification of the 23,000–year ice–volume cycle, *Science, 212*, 617–627, 1981.

Ruddiman, W. F., and A. McIntyre, An evaluation of ocean-climate theories on the North Atlantic, in *Milankovitch and Climate*, part 2, edited by A. Berger et al., pp. 671-686, Kluwer Acad., Norwell, Mass., 1984.

Sakai, K., and W. R. Peltier, Dansgaard-Oeschger oscillations in a coupled atmosphere-ocean climate model, *J. Clim., 10*, 949-970, 1997.

Saltzman, B., Three basic problems of paleoclimatic modeling: A personal perspective and review, *Clim. Dyn., 5*, 67–78, 1990.

Saltzman, B., and K. A. Maasch, Carbon cycle instability as a cause of the late Pleistocene ice age oscillations: Modeling the asymmetric response, *Global Biogeochem. Cycles, 2*, 177-185, 1988.

Saltzman, B., and A. Sutera, A model of the internal feedbacks system involved in late Quaternary climatic variations, *J. Atmos. Sci., 41*, 736-745, 1984.

Saltzman, B., and M. Y. Verbitsky, The late Cenozoic glacial regimes as a combined response to Earth-orbital variations and forced and free CO_2 variations., in *Ice in the Climate System, NATO Proceedings*, edited by R. Peltier, pp. 343-361, Springer-Verlag, New York, 1993.

Schmitt, R. W., The ocean fresh water cycle, *OOSDP Background Rep. 4*, Ocean Observing System Development Panel, 32 pp., 1994.

Stokes, W. L., Another look at the ice age, *Science, 122*, 815–821, 1955.

Stommel, H., Thermohaline convection with two stable regimes of flow, *Tellus, 13*, 224–230, 1961.

Stone, P. H., A simplified radiative-dynamical model for the static stability of rotating atmosphere, *J. Atmos. Sci., 29*, 405-418, 1972.

Suarez, M. J., and I. M. Held, Modeling climatic response to orbital parameter variations, *Nature, 263*, 46-47, 1976.

Taylor, K. C., G. W. Lamorey, G. A. Doyle, R. B. Alley, P. M. Grootes, P. A. Mayewski, J. W. C. White, and L. K. Barlow, The 'flickering switch' of late Pleistocene climate change, *Nature, 361*, 432-436, 1993.

Thorndike, A. S., A toy model linking atmospheric thermal radiation and sea ice growth, *J. Geophys. Res., 97*, 9401-9410, 1992.

Tziperman, E., Inherently unstable climate behavior due to weak thermohaline ocean circulation, *Nature, 386*, 592-595, 1997.

Tziperman, E., J. R. Toggweiler, Y. Feliks, and K. Bryan, Instability of the thermohaline circulation with respect to mixed boundary condition: Is it really a problem for realistic models?, *J. Phys. Oceanogr., 24*, 217-232, 1994.

UNESCO, 10th report of the joint panel on oceanographic tables and standards, *UNESCO Tech. Pap. in Mar. Sci. 36*, Paris, 1981.

Walsh, J. E., The role of sea ice in climatic variability: Theories and evidence, *Atmos. Ocean, 21*, 229-242, 1982.

Watts, R. G., and E. Hayder, A two-dimensional, seasonal, energy balance climate model with continents and ice sheets: Testing the Milankovitch theory, *Tellus, 36*, 120-131, 1984.

Weaver, A. J., M. Eby, A. F. Fanning, and E. C. Wiebe, Simulated influence of carbon dioxide, orbital forcing and ice sheets on the climate of the last glacial maximum, *Nature, 394*, 847-853, 1998.

Weertman, J., Milankovitch solar radiation variations and ice age ice sheet sizes, *Nature, 261*, 17–20, 1976.

Weinelt, M., M. Sarnthein, U. Pflaumann, H. Schultz, S. Jung, and H. Erlenkeuser, Ice-free Nordic seas during the last glacial maximum? Potential sites of deepwater formation, *Paleoclimates, 1*, 282–309, 1996.

H. Gildor and E. Tziperman, Environmental Sciences, Weizmann Institute of Science, Rehovot, 76100, ISRAEL. (e-mail: hezi.gildor@weizmann.ac.il; eli@beach.weizmann.ac.il).

(Received November 12, 1999; revised April 4, 2000; accepted June 24, 2000.)